Multi-Composition-EPSR: Towards Transferable Potentials To Model Chalcogenide Glass Structures.

James J. Towey and Emma R. Barney*

Faculty of Engineering, University of Nottingham, University Park, Nottingham, NG7 2RD

*Corresponding Author e-mail: Emma.Barney@nottingham.ac.uk

Telephone: +44 (0)115 74 84674

Abstract

The structure of $x As_{40}Se_{60}$-(1- x)$As_{40}S_{60}$ glasses, where x = 1.000, 0.667, 0.500, 0.333, 0.250 and 0.000, are investigated using a combination of neutron and X-ray diffraction coupled with computational modelling using Multi Composition Empirical Potential Structure Refinement (MC-EPSR). Traditional EPSR (T-EPSR) produces a set of empirical potentials that drive a structural model of a particular composition to agreement with diffraction experiments. The work presented here establishes the shortcomings in generating such a model for a ternary chalcogenide glass composition. In an enhancement to T-EPSR, MC-EPSR produces a set of pair potentials that generate robust structural models across a range of glass compositions. The structures obtained vary with composition in a much more systematic way than those taken from T-EPSR. For example, the average arsenic-sulfur bonding distances vary between 2.28-2.46 Å in T-EPSR but are 2.29±0.02 Å in MC-EPSR. Similarly, the arsenic-selenium bond lengths from T-EPSR vary between 2.28-2.43 Å but are consistently 2.40±0.02 Å in the MC-EPSR results. Analysis of these models suggests that the average separation of the chalcogen (S or Se) atoms is the structural origin of the changes in non-linear refractive index with glass composition.

1. Introduction

It has been widely reported that atomic scale oscillations of molecular bonds can strongly absorb specific wavelengths of light in the mid infra-red (mid-IR) region of the electromagnetic spectrum (3-12 μm). This means that the presence of compounds of interest can be identified, and quantified, by using spectroscopy to measure these absorptions, often referred to as "molecular fingerprints" [1-2]. Studies have shown that a wide range of organic molecules, from toxic agents [3] and greenhouse gasses [4] to biological tissue [5] and beer [6], can be identified using their characteristic molecular vibrations. Unfortunately, the current ability to exploit this spectroscopic technique is limited by the lack of off-the-shelf mid-IR optics [2]. New mid-IR sources, guides and detectors are required in order to harness the potential of mid-IR light for real-time, remote sensing [1]. In recent years, glass fibres based on chalcogen elements (S, Se and Te) have been proposed as prospective candidates for these technologies due to their ability to transmit, and interact with, mid-IR light [1-2, 7].

Chalcogenide glasses have long been known to possess optical properties that make them attractive potential materials for use in mid-IR spectroscopy applications [7]. They transmit light from 2-10 μm and possess a range of other favourable qualities, including good thermal stability and resistance to crystallisation, that facilitate the shaping and manufacture of the glass into fibres and waveguides. Furthermore, the broad concentration range over which chalcogenide glasses form offers exciting possibilities for tailoring properties via compositional development [7-10]. To successfully exploit $As_{40}Se_{60}$-$As_{40}S_{60}$ glasses as materials for mid-IR optical fibres it is necessary to be able to control the physical properties. Understanding the composition-structure-property relationships that govern this system would enable glasses with specific functional properties to be designed. However, fully exploring and characterising the glass forming regions is both time consuming and costly. As such, device development has been limited to a small number of glass compositions that are known to provide suitable functional properties. This investigation builds upon recent work carried out by the authors using a number of different structural techniques to characterise a series of stoichiometric $As_{40}Se_{60}$-$As_{40}S_{60}$ glasses [11]. The current work is motivated by the desire to build computational structural models of these glasses to understand the effect of composition on their short and medium range order. These models can then be used to explore the links between glass structure and macroscopic properties, investigating the validity of conclusions drawn by Barney *et al.* [11]. The ultimate goal is the development of a robust and reliable methodology for predicting the structure of a chalcogenide glass composition via computational modelling. Success would enable glass properties to be estimated from the structural motifs predicted, without the investment in time and resources to melt and characterise the glass. In this way, it would be possible to focus compositional development on areas of the glass forming region most likely to yield glasses with the desired properties.

A number of chalcogenide glasses have been studied using computational modelling, including two glass compositions of interest here, $As_{40}Se_{60}$ and $As_{40}S_{60}$ [8, 12-17]. Many of these computational studies have used Molecular Dynamics (MD) techniques. MD simulations aim to calculate the trajectory of the atoms of interest by solving Newton's equations of

motion. The movement of the atoms within the simulation is controlled by the interaction potentials that provide the force field. Broadly speaking, the different methods of calculating these force fields can be split in to two groups, classical and quantum mechanical (QM). Classical simulations use empirically derived force fields while QM simulations obtain the potentials directly from calculations of the Schrödinger equation associated with the system being studied. As a result, QM simulations are more computationally costly than classical MD, due to the level of calculation required, but can provide an interesting insight into the structure of small systems. There have been a number of studies in the literature using *ab initio* QM MD approaches to model $As_{40}Se_{60}$ and $As_{40}S_{60}$ in both amorphous [8, 12, 14-21] and liquid [16, 22-23] states. The models for these studies have ranged in size from 80 to 200 atoms, and the general consensus is that ~16% of Se bonds are homopolar. This is consistent with ^{77}Se MAS NMR results for $GeSe_2$ published by Gjersing *et al.* [24], but it is not consistent with the ^{77}Se MAS NMR results recently published by the authors for $As_{40}Se_{60}$ [11], which showed no peak arising from Se-Se bonds.

Another widely used simulation technique is the Monte Carlo (MC) method. MC simulations rely on random movement of the atoms in the simulation. These moves are then accepted or not based on criteria prescribed by the type of simulation that is being run. In standard MC studies the moves are accepted based on whether or not they lower the potential energy of the system. This technique was employed by Mauro and Varshneya [15], who used a combination of QM interatomic potentials and Metropolis MC simulations to study two arsenic selenide glass compositions. However, the success of this work was limited. The fraction of arsenic atoms that were 3 coordinated was only ~60%, with a correspondingly low number of 2 coordinated Se atoms (45%) [15]. Bauchy and Micoulaut later compared the published simulated structure factors with experimental data to show poor agreement [12]. The lack of agreement between simulation and experiment is a major drawback for both MD and standard MC studies. Indeed, it is often sufficiently poor that the results are unconvincing [8, 15] and too disparate to allow competing structural models to be tested reliably [17]. In some cases the simulations are not tested against experimental data at all [16].

One way to avoid the problem of inconsistency between simulation and experiment is to use methods such as Reverse Monte Carlo (RMC). Unlike the simulation techniques outlined above, RMC does not require appropriate interatomic potentials to produce the simulation. Instead, a trial and error method of modifying the atomic coordinates is used and movements are accepted based on whether or not they improve the agreement of the simulation with experimental data [25]. The lack of interatomic potentials dramatically reduces the computational time required to perform these simulations and allows significantly larger simulation sizes to be conducted than are possible with other simulation studies. Typical simulation boxes will contain between 5,000 [13] – 20,000 [14] atoms. Previous RMC simulations of chalcogenide glasses have had mixed success. Fabian *et al* [26] studied $As_{40}Se_{60}$ glasses and found that both the arsenic and selenium atoms have lower average coordination numbers than expected; 2.6 and 1.8 rather than 3 and 2. However, Kaban *et al* [14] had more success simulating $As_{40}S_{60}$ glasses, obtaining coordination numbers of 2.94 (As) and 1.96 (S). To our knowledge, RMC has not been used previously to study ternary As-S-Se glasses. The lack of interatomic potentials in RMC makes it difficult to ensure consistency between models of different glass compositions, as each simulation is entirely independent. This is of particular importance when the interatomic interactions that drive the glass structure are of interest. For example, it has been previously shown that the charge density associated with lone-

pair electrons, such as are found on arsenic atoms, are crucial for understanding glass structures and functional properties [27-28]. A further drawback for this modelling method is that it is reliant on experimental data and cannot be used to predict the structure of new glass compositions.

This study seeks to use a simulation technique, Empirical Potential Structure Refinement [29] (EPSR), which provides a structure that is consistent with the experimental results, and allows inter-atomic potentials to be included. EPSR is a form of RMC simulation, which uses inter-atomic potentials to produce an approximate model of the system. These potentials are then iteratively modified until agreement between the simulation and experimental data is reached. EPSR has traditionally been used to probe aqueous systems, where contrast from isotopic H/D substitution can be easily obtained to help guide the simulation to chemically reasonable solutions [30]. There have, however, been several proof of concept studies of glass structure [27, 31-35]. Of particular note is the work of Soper [33], who investigated the presence of homopolar Se-Se bonds in $GeSe_2$, and Alderman *et al.* [27] who used dummy lone-pair atoms to simulate steric environments for lead atoms in a $PbO\text{-}SiO_2$ glass. In the present study, EPSR has been used to probe the structure of stoichiometric $As_{40}Se_{60}$-$As_{40}S_{60}$ glasses. This is the first report to systematically develop computational models for a series of chalcogenide glasses across a compositional range (in this case $As_{40}Se_{60}$ to $As_{40}S_{60}$). To produce chemically reasonable structural models, the investigation has built upon the work of Soper [33] and Alderman *et al.* [27] but has implemented a new methodology for EPSR which builds a single set of potentials that are consistent with all the data sets available.

The remainder of the article is structured as follows. Section 2 describes the methodology that was employed to study arsenic-sulfur-selenium glasses. Here, the problems of using traditional Empirical Potential Structure Refinement (EPSR) are highlighted, and the relative merits of using Multi-Composition EPSR (MC-EPSR) are demonstrated. Section 3 details and discusses the results for an MC-EPSR study of arsenic-sulfur-selenium glasses. In particular, the effect of using dummy lone-pair atoms (c.f. Alderman *et al.* [27]) is investigated. Section 4 concludes.

2. Methodology

2.1. Sample preparation and characterisation

A series of xAs$_{40}$Se$_{60}$-(1- x)As$_{40}$S$_{60}$ glasses where x = 1.000, 0.667, 0.500, 0.333, 0.250 and 0.000 (see Table 1) have been included in this study and the sample preparation and characterisation have previously been reported by Barney *et al.*[11]. The neutron structure factors presented here were measured using the GeM diffractometer [36] at the ISIS Pulsed Neutron and Muon Source (Rutherford Appleton Laboratory, Oxfordshire, UK). The data were collected for as-annealed glass rods held inside cylindrical vanadium containers, of inner diameter 10 mm. These vanadium containers were thin-walled, with a thickness of 25 µm, in order to reduce the magnitude of the experimental corrections required. Gudrun [37] and ATLAS [38] software were used to normalise the data using a calibration measurement of an 8 mm vanadium rod. The data were also corrected for attenuation, multiple scattering and scattering from the sample container and the empty instrument to give the distinct scattering spectra, $F^{\mathrm{N}}(Q)$. $F^{N}(Q)$, is given by the summation of the partial structure factors, $S_{\alpha\beta}(Q)$, weighted by the concentration, c, and scattering length, b, of the relevant pair of atoms α and β.

$$\boldsymbol{F^{N}(Q) = \sum_{\alpha\beta} c_{\alpha}\, c_{\beta} b_{\alpha} b_{\beta} \left(S_{\alpha\beta}(Q) - 1\right)} \quad (1)$$

The X-ray data were collected at the Diamond Light Source (Rutherford Appleton Laboratory, Oxfordshire, UK) using the I15 beamline optimised for the collection of PDF data. The photon energy used for the experiment was 73 keV. The samples were powdered and placed in 1 mm diameter silica capillaries, and the scattering was detected using a Perkin Elmer 2D flat panel 1621 detector. The 2D data were reduced to 1D using Fit2D [39-40] and were corrected for detector attenuation following the method detailed by Skinner *et al.* [41]. The 1D data were normalised using the Krohe-Moe and Norman method [42-43] and corrected for attenuation, multiple scattering and scattering from the sample container and the empty instrument using GudrunX [44] to produce the sharpened distinct scattering spectra, $F^{\mathrm{X}}(Q)$. In an analogous manner to $F^{\mathrm{N}}(Q)$, $F^{X}(Q)$ is defined as,

$$\boldsymbol{F^{X}(Q) = \sum_{\alpha\beta} c_{\alpha}\, c_{\beta} f_{\alpha}(Q) f_{\beta}(Q) \left(S_{\alpha\beta}(Q)\right)} \quad (2)$$

where, $f_{\alpha}(Q)$ is the atomic form factor for atom α. All the EPSR fits were made to $F^{\mathrm{N}}(Q)$ and $F^{\mathrm{X}}(Q)$. However, for ease of interpretation, the results have been shown in real-space. To achieve this, $F^{\mathrm{N}}(Q)$ and $F^{\mathrm{X}}(Q)$ were Fourier transformed using the Lorch modification function [45] and a maximum momentum transfer, Q_{max}, of 35 Å^{-1} for neutron and 25 Å^{-1} for X-ray data. This yielded the total radial distribution functions, $G(r)$, defined as,

$$\boldsymbol{G(r) = \sum_{\alpha\beta} c_{\alpha}\, c_{\beta} a_{\alpha}(Q) a_{\beta}(Q) \left(g_{\alpha\beta}(r) - 1\right)} \quad (3)$$

where $a_{\alpha}(Q)$ is either the neutron scattering length, b, or the X-ray atomic form factor, $f_{\alpha}(Q)$, for atom α and $g_{\alpha\beta}(r)$ are the partial radial distribution functions. The coordination numbers ($n_{\alpha\beta}$) are calculated from the relevant partial RDFs ($g_{\alpha\beta}(r)$) using the following equation,

$$n_{\alpha\beta} = 4\pi\rho c_\beta \int_{r_{min}}^{r_{max}} r^2 g_{\alpha\beta}(r) dr \quad (5)$$

where ρ is the atomic number density of the system, c_β is the proportion of atoms of type β in the system and r_{min} and r_{max} are the radial limits of the integration. To extract coordination numbers for arsenic, sulfur and selenium nearest neighbours, r_{min} values were set to 1.00 Å and r_{max} was defined as the position of the minimum following the first peak in the relevant partial RDF (2.79-2.88 Å for each of the As-S and As-Se correlations studied). The average arsenic-chalcogen coordination number, n_{AsCh}, for a particular composition is given by the sum of n_{AsS} and n_{AsSe} while the chalcogen-arsenic coordination number, n_{ChAs}, is calculated as,

$$n_{ChAs} = (X \cdot n_{SeAs}) + ([1 - X] \cdot n_{SAs}) \quad (6)$$

A key factor to consider when producing simulations for glass structures based upon scattering data is the scattering lengths of the atoms in the system. The total scattering functions (Equations (1) and (2)) are comprised of a weighted sum of all of the pair correlations found in the glasses. In the neutron measurement the scattering lengths, b, of arsenic, sulfur and selenium are 6.58, 2.85 and 7.97 fm respectively, while the X-ray form factors ($f_\alpha(0)$) are 33, 16 and 34. In both cases, the signals from the Se correlations are much stronger than from S correlations, giving little contrast between the two techniques. To compensate for the weak scattering from sulfur, an extra, sulfur-rich, sample (x=0.250) was included in the analysis to give an asymmetric concentration series (Table 1).

2.2. EPSR methodology

EPSR is a form of Monte Carlo simulation that utilises an iterative algorithm to produce a 3-dimensional atomic structure consistent with experimental diffraction data [29, 46-48]. Traditionally, EPSR has been used to investigate aqueous systems (see for example [30, 49]); however ionic liquids [50] and glassy systems [27] have also been studied. This versatility is achieved due to EPSR being a purely structural technique. The dynamical properties of the models are not considered and, therefore, a glass is essentially indistinguishable from a liquid sample. To simulate a structure, an initial interatomic reference potential, U^{ref}, for each atom pair present is required. These take the form of a combination of a Lennard-Jones and Coulomb term and are defined as,

$$U^{ref}(r_{ij}) = 4\epsilon_{\alpha\beta}\left[\left(\frac{\sigma_{\alpha\beta}}{r_{ij}}\right)^{12} - \left(\frac{\sigma_{\alpha\beta}}{r_{ij}}\right)^{6}\right] + \frac{q_\alpha q_\beta}{4\pi\epsilon_0 r_{ij}} \quad (4)$$

here, $\sigma_{\alpha\beta}$ and $\epsilon_{\alpha\beta}$ are standard Lennard-Jones parameters, q_α is the charge on atoms of type α and $\epsilon_0$is the permittivity of free space. The atomic potentials, formulated from the values shown in Table 2, were combined using Lorentz-Berthelot mixing rules to yield the appropriate interatomic potential. The reference potentials used in EPSR are often taken from the literature. This procedure has been employed for many different systems and details can be found elsewhere [29-30, 46, 49-52].

2.3. Determining starting potentials, U^{ref}.

Literature potentials were not used as a starting point for the present study because they were not deemed to be consistent with structural measurements (e.g. [8, 15]). Therefore, initial interatomic potentials for As, Se and S were obtained via a trial and error approach. The selected parameters, given in Table 2, were chosen to reproduce the first peak positions in the total radial distribution functions ,$G(r)$, after thermalisation. This approach has previously been applied successfully to simulate the structure factors for lead silicate [27] and germanium selenide [48] glasses. As shown in Figure 1a, the final structural model reproduces the position of the first peak in $G(r)$ at ~2.35 Å but fails to reproduce the data at longer distances. In addition to simulating the correct bond lengths, the results were also required to be consistent with the spectroscopic results from a recent study of $As_{40}Se_{60}$-$As_{40}S_{60}$ glasses [11]. Barney *et al.* used Raman spectroscopy to show the lack of S-S bonding and ^{77}Se NMR studies to show that the selenium atoms are mainly found in [$AsCh_3$] units [11]. To enforce the absence of homopolar bonds, minimum approach distances (Rmin values, given in Table 3) were included in the reference potentials.

2.4. Traditional EPSR simulation of $As_{40}Se_{60}$-$As_{40}S_{60}$ glasses and the need for a new technique

Initial models for the six $As_{40}Se_{60}$-$As_{40}S_{60}$ glasses were generated using T-EPSR. The first stage of the procedure was to carry-out an energy minimisation of simulation boxes containing 5,000 atoms in the correct ratio of As, Se and S for each composition (Table 1). Then, using the finalised values for U^{ref} (Table 2), a thermalisation was performed for each of the glass compositions individually. The simulated structure factors for each composition were then compared to the corresponding experimental $F^{\mathrm{N}}(Q)$ and $F^{\mathrm{X}}(Q)$. To minimise the difference between the simulated RDFs and the experimental data a set of empirical terms were generated to modify U^{ref}. In this way, an iterative refinement to the inter-atomic interactions was made for each composition; additional empirical potentials were applied to the atom potentials until an optimised agreement between model and experiment was achieved for each individual composition (see **Scheme 1**). The effect of modifying U^{ref} with empirical potentials can be appreciated by comparing the initially simulated neutron and X-ray radial distribution functions, $G(r)$, for $As_{40}Se_{30}S_{30}$ in Figure 1a with the refined $G(r)$s for the same composition, shown in Figure 1b. In the latter, the simulated $G(r)$s more fully reproduce the experimental $G(r)$s on all length scales. A similar quality of fit was found for each composition (see Supplementary Information, Figure S1). Once this level of agreement is achieved is it possible to interrogate an ensemble of atomic structures that are consistent with the experimental data for insights into the glass structure [29].

An initial analysis of the six simulations produced using T-EPSR was performed by examining the first peaks in the As-Ch partial radial distribution functions, $g_{\mathrm{AsCh}}(r)$. All the As-Ch partials are shown in Supplementary Information, Figure S2. The positions of the first $g_{\mathrm{AsCh}}(r)$ peaks for the binary glasses, 2.28 Å and 2.40 Å for $As_{40}S_{60}$ and $As_{40}Se_{60}$ respectively, were consistent with previous X-ray diffraction studies of $As_{40}S_{60}$ (2.26 Å [14]) and $As_{40}Se_{60}$ (2.42 Å [26]) glasses and were verified using bond valence calculations [53], which yielded an As-S bond length of 2.26 Å and an As-Se bond

length of 2.39 Å. However the peak positions obtained for the ternary glasses were unsatisfactory. Figure 2a shows the simulated nearest neighbour peaks for the arsenic-sulfide (As-S; black dashed line) and arsenic-selenide (As-Se; red dashed line) correlations in $As_{40}S_{30}Se_{30}$ along with dotted lines corresponding peak positions for the As-S and As-Se bond lengths found in the simulations of $As_{40}S_{60}$ and $As_{40}Se_{60}$. The positions of the As-S and As-Se peaks in $As_{40}S_{30}Se_{30}$ are representative of $g_{\mathrm{AsCh}}(r)$ for all four ternary glasses s, having an As-Se bond length (2.28-2.37 Å) that is shorter than the As-S bond (2.34-2.46 Å), in direct disagreement with the bond lengths extracted from the simulations for $As_{40}S_{60}$ and $As_{40}Se_{60}$ glasses. Therefore, the simulations produced using T-EPSR for the ternary glass compositions were inconsistent with both the simulations for the binary glasses and the chemical understanding of As-Se and As-S bonds. In conclusion, T-EPSR was not sufficiently constrained by the combination of diffraction data and reference potentials to yield refined reference potentials able to produce reliable structures for individual ternary glasses.

2.5. Development of the Multi-Composition EPSR methodology

To successfully generate physically reasonable models for the $As_{40}Se_{60}$-$As_{40}S_{60}$ glass system, it was necessary to increase the number constraints on the simulations. When considering potential methods to introduce new constraints to the data, it was noted that EPSR was able to simulate As-Ch bond lengths for $As_{40}S_{60}$ and $As_{40}Se_{60}$ that were consistent with bond valence calculations. Therefore, it would be advantageous to incorporate the atomic potentials refined for these two glass compositions into the simulations for the more complex ternary glasses. The methodology used to achieve this, Multi-Composition EPSR (MC-EPSR), is shown in **Scheme 2**. The aim of MC-EPSR is to produce a single set of empirically derived pair potentials which generate simulations consistent with experimental data for a range of glass compositions (i = 1 to n). This is accomplished by using the difference between the experimental and simulated structure factors for composition i to modify the potentials for composition i + 1. The difference between the simulation and experimental data for composition i + 1 is then used to modify the potentials for concentration i + 2 and so on. By iterating this procedure cyclically, an equilibrium is reached in which a) each individual structure factor is successfully simulated by MC-EPSR while b) ensuring that the As-S and As-Se bond lengths in every simulation are consistent with those measured experimentally for the binary glasses. In this way, MC-EPSR produces a single set of potentials that are able to produce structures consistent with experimental data for any composition across those studied.

MC-EPSR was run twice for the data sets in the $As_{40}Se_{60}$-$As_{40}S_{60}$ system using two different configurations. The first configuration, hereafter referred to as the Atomic configuration, contained 5,000 atoms and were composed of a mix of As, Se and S atoms. The second configuration, henceforth referred to as the Lone Pair configuration, contained an additional 2,000 dummy atoms used to simulate the lone pair of electrons associated with each arsenic atom [27]. These dummy atoms, called q atoms in EPSR, do not contribute mass to the system or alter the number density of the box. Furthermore, they have zero scattering length, and so do not result in features in the scattering pattern. However, each one is tied to an arsenic atom to form a q-As' molecule with a separation distance of 0.7 Å, which is held constant using a large intermolecular potential energy.[27] The presence of a q atom next to each of the As atoms prevents other

As, Se and S atoms entering that volume to simulate the steric effect of the lone-pair of electrons. The reference potentials, listed in Table 2, for Se and S were identical in the two approaches, but the coulomb charge for As was altered in the lone pair configuration (As') to accommodate the negative charge associated with the lone pair atom (qAs). The minimum approach distances for all the atoms are given in Table 3 and have been set to ensure that the models contain no homopolar bonds. The final fits to the structure factors, along with the As-Ch partial radial distribution functions, $g_{\mathrm{AsCh}}(r)$, are given in the Supplementary Information (Figure S3-S6) for all compositions in both configurations. Visual inspection of each $G(r)$ shows little difference in quality of fit with that in Figure 1b. However, inspection of $g_{\mathrm{AsCh}}(r)$ show significant differences between the MC-EPSR simulations and those generated by T-EPSR.

The $g_{\mathrm{AsCh}}(r)$s taken from the atomic MC-EPSR analysis of the $As_{40}S_{30}Se_{30}$ structure are shown in Figure 2b and are representative of the results obtained for all ternary compositions and both configurations (see Supplementary Information, Figure S4 and S6). In contrast to $g_{\mathrm{AsCh}}(r)$in Figure 2a, the average arsenic-sulfur bond length (as indicated by the position of the peak in $g_{\mathrm{AsS}}(r)$) was at a shorter distance than the arsenic-selenium bond length in $g_{\mathrm{AsSe}}(r)$. The first peaks in $g_{\mathrm{AsS}}(r)$and $g_{\mathrm{AsSe}}(r)$were at 2.28 Å and 2.40 Å, coinciding with the positions of the first peaks in $G(r)$ for $As_{40}S_{60}$ and $As_{40}Se_{60}$ respectively (dotted lines). In conclusion, the obvious difficulties in obtaining accurate local structural information for systems with insufficient experimental constraints have been obviated by the use of MC-EPSR, which ensures that the arsenic-chalcogen bond lengths in all the simulated glass structures for the $As_{40}Se_{60}$-$As_{40}S_{60}$ system were consistent with diffraction experiments [11, 14, 26] and bond valence calculations [53]. The rest of this paper will compare and discuss the results obtained using the Atomic and Lone-Pair configurations to determine the reliability of the models obtained and draw conclusions about the structure of the glasses.

3. Results and Discussion

3.1. A comparison of MC-EPSR models generated using atomic and lone pair simulations.

3.1.1 Coordination numbers

Figure 3 shows the average As-Ch coordination numbers, n_{AsCh}, for each composition simulated using MC-EPSR with Atomic (Figure 3a) and Lone-Pair (Figure 3b) configurations. Figure 3a shows that values for n_{AsCh} obtained using the Atomic configurations vary between 3.08 and 3.24, with higher values of n_{AsCh} found in sulfur rich glasses (n_{AsCh}> 3.20 at $x \leq 0.500$). The individual As-Ch coordination numbers, n_{AsS} and n_{AsSe}, shows that this over-coordination arises from As-S bonds. n_{AsS} is consistently higher than expected, while n_{AsSe} is slightly lower. In contrast, Figure 3b shows that the average values of n_{AsCh} obtained using the Lone-Pair configuration are much closer to the expected value of 3, varying between 2.97 and 3.00.

An alternative analysis of the coordination numbers can be obtained by considering the distribution of coordination environments in the glass. Table 4 shows that attaching a dummy lone pair atom to each arsenic atom reduces the standard deviation on the average arsenic coordination number for $As_{40}Se_{60}$ from 0.71 to 0.27, with a corresponding improvement also observed for $As_{40}S_{60}$. Table 5 and figure 4a show this difference in standard deviation arises from the greater variation in the arsenic environment in the Atomic configurations. Across all the glass compositions, only 50-54 % of the arsenic atoms are coordinated by 3 chalcogen atoms in the Atomic configuration with 28-37 % of the As atoms bonded to 4 chalcogens and the remaining 11-17 % have a coordination number less than 3. In contrast, in the Lone-Pair simulations, 88-92 % of the arsenic atoms are 3 coordinated and the remaining As atoms are evenly divided between 2 and 4 coordination environments, resulting in the average coordination number of ~ 3. An analysis of the structure of crystalline As_2Se_3 [54] and As_2S_3 [55] shows that only [$AsCh_3$] units are likely to be present in these glasses, and this is corroborated by the position and width of the As-Ch peaks fitted to the data in a previous study [11].

A consideration of the change in the average chalcogen-arsenic coordination number, n_{ChAs}, across the six glass compositions shows similar trends to those outlined above for the arsenic environments. Figure 3c indicates that the sulfur atom environments obtained from the Atomic configuration are significantly “over-coordinated” in the ternary glasses, with an average of 2.14-2.37 arsenic atoms in the first coordination shell. In contrast, the selenium atoms are only slightly under-coordinated (n_{SeAs} =1.92-2.05), resulting in an average n_{ChAs} that is greater than two. Figure 3d shows that the n_{ChAs} values obtained from the Lone Pair configuration are much closer to the expected value of 2 for each composition, varying between 1.98- 2.02, although the n_{SAs} is still higher than expected in the ternary glasses, and n_{SeAs} is lower.

To explain these results, it can be postulated that the weak scattering from sulfur atoms, resulting in a lack of intensity in the structure factor from sulfur correlations, coupled with no method for enforcing the "voids" near the [$AsCh_3$] units that arise from the presence of a lone pair, allows sulfur atoms to cluster around the arsenic atoms in higher concentrations than expected without significantly altering the simulated structure factor. By reproducing the effect of a lone pair using a dummy atom, the available space for additional chalcogens to cluster around arsenic is greatly reduced. However, while the addition of the lone pair atoms has greatly reduced the distribution of As environments, the change in the Se environment induced by including lone pair atoms is minimal.

3.1.2 Bond Angle Distributions

The structural differences between the MC-EPSR simulations carried out with and without dummy lone pair atoms can be further explored by investigating the Ch-As-Ch bond angles within the [$AsCh_3$] polyhedra. There is remarkable consistency in the shape of the distributions observed for each glass composition generated using a particular configuration. The distribution of bond angles obtained for simulations using the Atomic configuration are shown in Figure 5a and have a bi-modal distribution, with a sharp peak at 95° and a much broader peak at 145°. An evaluation of the mean and modal averages of the angular distributions, shown in Figure 5 b, yields values of ~109° and ~96° respectively, across the compositional range. The mean bond angle is close to that expected for an [$AsCh_4$] tetrahedron and this may be reflective of the increased number of 4 coordinated units in the atomic simulations. It is worth noting that Alderman *et al.*[27] also observed a bimodal distribution of O-Pb-O bond angles in the atomistic models of 80PbO-20SiO_2 glass. Following the work of Alderman *et al.,* the lone pair configuration was expected to reduce the width of the bond angle variation in the simulation.

Figure 5c shows that the addition of a lone pair to each As atom has the effect of sharpening the bond angles distribution in the Ch-As-Ch triplets, removing the shoulder, and producing a unimodal peak centred at ~94° with mean and modal averages that are in close agreement (~94° and ~93° respectively Figure 5 d). This is very close to the X-As-X bond angles reported by Gillespie [56] for lone pair molecules, AsF_3 and $AsCl_3$ (95.8° and 98.9° respectively). The Ch-As-Ch bond angle distribution in crystalline As_2S_3 and As_2Se_3 ranges from 90.6° to 106.5°. The mean median and modal average angles are 98.85°, 98.65° and 98.7° respectively with a standard deviation of 5.2°. Therefore, the unimodal shape of the Ch-As-Ch bond angle distributions generated by the Lone-Pair configuration match that found in the crystal structures, but the average bond angles are ~4° smaller. The current work has been more successful in producing the expected single Gaussian distribution with closely matched mean and modal values than that of Alderman *et al.*[26] and this difference may be a result of the much wider variation in Pb environments found in lead oxide glasses, where a range of different coordination environments are known to exist.[57]

A consideration of the As-Ch-As bond angle distributions obtained using the Lone-Pair configurations (See supplementary information Figure S7) show that there is a bimodal distribution of angles in all the models, with a peak maximum at ~97° (95° in the selenide glass, shifting to 101° in the sulphide glass) and a shoulder at ~140°. A bimodal distribution is also observed in the crystalline analogues of As_2S_3 and As_2Se_3 centred at ~101°, however the distribution

is significantly narrower. The mean, median and modal averages for the As-Ch-As bond angle distribution in the crystals are 97.0°, 99.5° and 101° respectively, with a standard deviation of 6.4°. Therefore the shoulder at 140° observed in the Lone-Pair model is considered to be unphysical.

3.1.3 The chalcogen environment.

Figure 3b, Figure 4a and Figure 5c show the marked effect attaching dummy lone pair atoms to the arsenic atoms has on the distribution of As-Ch environments. In contrast, Figure 4b (and the similarity between Figure 5a and Figure S7) shows that there is little difference in the selenium environments found in the Atomic and Lone-Pair configurations. A significant number of 0, 1, 2 and 3 coordinated Se present in both models along with a significant number of As-Ch-As bond angles of ~140°. The presence of a dummy lone pair atom in the local environment of arsenic fills space, preventing more than three chalcogen nearest neighbours, thereby constraining the number of lower coordination environments that may form to maintain an average coordination number of 3, and reducing the range of As-Ch-As bond angles. However, there is no such constraint on the selenium environment. The authors postulate that a similar reduction in the distribution of Ch environments may be achieved if the two lone pairs of electrons on the S and Se atoms were are also included in the model. However, this would add 50% more spheres to the lone pair simulation and significantly increase the computational time required. A more elegant method of controlling the local environments of atoms would be to add a coordination number or bond valence constraints and this is future work to develop MC-EPSR.

3.2. A comparison of the partial correlation functions simulated using Lone-Pair MC-EPSR with crystalline As_2Se_3.

An important test for any atomistic model is to examine the partial structure factors to ensure that the model is chemically reasonable. Figure 6 plots the three partial structure factors, As-As, As-Se and Se-Se, obtained for the $As_{40}Se_{60}$ sample using Lone-Pair MC-EPSR with those simulated for crystalline $As_{40}Se_{60}$. The XTAL program [58] was used to simulate the partials correlation functions for the crystal using the published atomic positions and lattice parameters.[59] The ideal partial correlation functions were broadened for the effects of real space resolution (arising from a finite Q_{max}) and thermal motion. For longer distances, the rms variation in interatomic distance was calculated from the published anisotropic thermal parameters, but for short distances (i.e. As-Se bonds and Se…Se nearest neighbours) the values taken from fitting the correlation functions for amorphous As_2Se_3 were used, simulating the effects of correlated motion. [11]

A direct comparison of the partial correlation functions simulated using Lone-Pair MC-EPSR with the simulated partial correlation functions for the crystal shows excellent agreement between the two. The position of the first peak in each partial produced by the atomistic model matches that found in the crystal, and there is also good agreement between the positions of the second peaks in the partials for each interatomic pair. Unlike the crystal data, the partial correlation functions simulated for the glass have very few features beyond 6 Å. This is expected, due to the

amorphous nature of the material, and the good agreement between crystal and simulated glass structure over the short range indicates that the model for $As_{40}Se_{60}$ is chemically reasonable. Figure S8 in the supplementary information shows the partial correlation functions for $As_{40}Se_{60}$ with those of $As_{40}Se_{30}S_{30}$ and $As_{40}S_{60}$ to demonstrate that there the partials generated for each glass composition are consistent with each other.

3.3. A comparison of the MC-EPSR lone pair model for $As_{40}Se_{60}$ with MD simulations.

As stated in Section 1, this study is, to the best of our knowledge, the first to systematically sample across a series of chalcogenide glass compositions to produce consistent computational structural models. Furthermore, while there are numerous reports in the literature for structural models of $As_{40}Se_{60}$ [8, 12, 15, 18, 20, 23], we are unaware of any studies of As-Se-S glasses due to the difficulties discussed in section 2. A comparison of As and Se environments generated by MC-EPSR using Atomic and Lone-Pair configurations has demonstrated that the presence of a lone pair atom associated with each arsenic atom markedly improves the quality of the model. However, before the structural simulations obtained for each of the glasses in the x $As_{40}Se_{60}$ – (1-x) $As_{40}S_{60}$ series can be studied in detail, it is necessary to ensure that the results obtained in this work are comparable in quality to the best MD simulations reported in the literature. [12 18]

The majority of reports for the structure of $As_{40}Se_{60}$ have used small box *ab initio* MD simulations with varying levels of success. Figure 4 compares the distribution of arsenic and selenium coordination numbers in the MC-EPSR atomic and lone pair simulations for $As_{40}Se_{60}$ with those reported in the literature [18 12 15]. Bauchy and Micoulaut's 2013 paper [12] directly compared the structural models for $As_{40}Se_{60}$ published by of Mauro and Varshneya [15], Li and Drabold [18] and Bauchy and Micoulaut [12] with experimental data to determine the quality of the three models. It was shown that the Bauchy and Micoulaut and Li and Drabold models both obtained similarly good quality of fits to the experimental data published by Salmon *et al.* [60]. However, the model proposed by Mauro and Varshneya failed to reproduce the intensity or positions of the peaks in the experimental structure factor. Indeed, Figure 4 shows that the Mauro and Varshneya model is of similar quality to the Atomic model reported here, with both simulations contain 1, 2, 3 and 4 coordinated arsenic atoms, low fractions of two-coordinated selenium, and a maximum bond angle distribution significantly different from that expected for the pseudo-trigonal bipyramid shape induced by the presence of a lone pair [56]. Due to the shortcomings of the Atomic and Mauro and Varshneya models for $As_{40}Se_{60}$, the discussion will now focus on the Lone-Pair model and those reported by Li and Drabold [18] and Bauchy and Micoulaut. [12]

Figure 7a shows the experimental $F^{\mathrm{N}}(Q)$ for $As_{40}Se_{60}$ reported by Barney *et al*. [11] along with the structure factor generated using the MC-EPSR lone pair configuration in this study and the corresponding simulated structure factor published by Bauchy and Micoulaut [12]. As might be expected, there is a significantly better agreement between the lone pair simulation and experiment than between experiment and the simulation of Bauchy and Micoulaut because the former is refined to give the best possible fit the experimental data. The major differences between the

experimental $F(Q)$ and the Bauchy and Micoulaut structure factor are the lack of a first sharp diffraction peak (FSDP) at ~1.25 $Å^{-1}$ in the model, and the reduced heights of the peaks at ~2.2 and ~3.4 Å compared to the experimental data. Inspection of the partial structure factors calculated from the lone pair simulation for $As_{40}Se_{60}$, suggests that the FSDP arises from a mix of As-Se and As-As correlations in the glass (see supplementary information). The effect of these differences in the structure of the glass can be best understood by inspecting the total radial distribution functions, $G(r)$ (Figure 7b). The data of Bauchy and Micoulaut are in agreement with the area of the experimental first peak, yielding an arsenic coordination number of 3.02 [12], but the peak maximum is at a longer distance (2.46 Å) than found experimentally (2.41 Å). Discrepancies can also be seen in the position of the second peak in $G(r)$, which is centered at 3.65 Å in the experimental data and at the longer distance of 3.73 Å in the simulation of Bauchy and Micoulaut[12]. It is non-trivial to assign the shift in this peak to a single atomic pair correlation because this region is composed of intensities from the $g_{\mathrm{AsAs}}(r)$, $g_{\mathrm{SeSe}}(r)$and $g_{\mathrm{AsSe}}(r)$ partials. However, the long As-Se bonds predicted by the simulation would be expected to have the effect of expanding the network structure and lengthen distances to all coordination shells. In summary, by refining the initial starting potentials used by EPSR, the structural models reported in this study are, unsurprisingly, in much closer agreement with experimental data than those generated from interatomic potentials alone.

Figure 4c compares the arsenic environments in the lone pair simulation for $As_{40}Se_{60}$ with those reported by Li and Drabold [18] and Bauchy and Micoulaut [12]. All three simulations indicate that between 89 and 97 % of As atoms are three-coordinated. However, in the Bauchy and Micoulaut simulation the majority of the remaining As atoms (9.7%) have more than 3 neighbouring atoms, resulting in an average arsenic coordination number that is >3. In the MC-EPSR lone pair and Li and Drabold simulations, the distribution of the remaining As atoms is evenly split between 2 and 4 coordination. In contrast, the selenium environments reported in Figure 4d, indicate that the Bauchy and Micoulaut simulation for $As_{40}Se_{60}$ is more realistic because 94% of the selenium atoms are two-coordinated; the Li and Drabold and lone pair simulations only achieve ~65% two coordinated Se atoms. Using this analysis, each of the models has it's own strengths in producing a chemically reasonable model. However, it should be remembered that an additional set of constraints were applied to this study. Spectroscopic studies of stoichiometric $As_{40}Ch_{60}$ glasses have suggested that the structure is predominantly comprised of [$AsCh_3$] pyramidal units [11, 61]. Therefore, the arsenic atoms are expected to be primarily coordinated by three chalcogen atoms (S and/or Se) while chalcogen atoms are coordinated by two arsenic atoms. Previous studies in the literature [12, 18] have not enforced the absence of homopolar bonds. Bauchy and Micoulaut reported that 21% of As bonds are to other arsenic atoms [12], while Li and Drabold found that 23% of As bonds were homopolar [18]. These values are ~three times greater than the 7% As-As bonds predicted by Georgiev [62] following analysis of Raman spectra for $As_{40}Se_{60}$, and ^{77}Se NMR work published by the authors show that the number of Se-Se bonds present in this $As_{40}Se_{60}$ sample is negligible. To incorporate the NMR results, this work has used minimum approach distances that ensure only As-S or As-Se bonds are possible in the final simulations. The excellent level of agreement between the MC-EPSR lone pair simulation for $As_{40}Se_{60}$ and experimental data, coupled with As and Se environments that are of comparable quality to those obtained by Li and Drabold [18] and Bauchy and Micoulaut

[12], demonstrates that it is possible to build a model for the structure of $As_{40}Se_{60}$ that does not require homopolar bonds to generate a high quality structural model for $As_{40}Se_{60}$.

In summary, a comparison of the lone pair model for $As_{40}Se_{60}$ with MD simulations reported in the literature indicates that the quality of the results are comparable, even with the addition of closest approach constraints to remove homopolar bonding in the current model. However, the truly unique aspect of this work is that rather than focusing on modelling one or two glass compositions individually, a single set of potentials has been derived that is capable of generating fits to 6 different compositions simultaneously. The success of this approach suggests that the final interatomic potential could be used predictively, to generate the structure of a previously unmeasured glass composition reliably.

3.4. Model Transferability

The MC-EPSR methodology, which combined with a lone pair starting configuration, has allowed structural models to be calculated for six glasses in the $xAs_{40}Se_{60} – (1\text{-}x)As_{40}S_{60}$ system (where x = 0.000, 0.250, 0.333, 0.500, 0.667 and 1.000) simultaneously. Furthermore, the agreement between simulation and experimental data (see S.I. Figs 3 and 5) is excellent, and the simulations all yield chemically reasonable models composed of ≥ 87% [$AsCh_3$] units (Table 4). However, all of these simulations were produced with reference to experimental data, and so the method is not intrinsically predictive. In contrast, Bauchy and Micoulaut were able to use the MD methodology to simulate structures for $As_{40}Se_{60}$ and $As_{20}Se_{80}$ [12] with no reference to experimental results at all. In order to investigate the transferability of the interatomic potentials generated using MC-EPSR with a lone-pair configuration, a subsequent neutron diffraction experiment was conducted on a glass with the composition x = 0.750 ($As_{40}S_{15}Se_{45}$). This composition was made using the same method as the other glasses investigated here [11].

Figure 8 shows the total radial distribution function, $G(r)$, from this experiment (red line) along with a predicted $G(r)$ (black dotted line) produced using the empirical potentials obtained from the MC-EPSR lone pair configuration. In previous EPSR studies the quality of fit between the experimental ($F_i(Q)$) and simulated ($D_i(Q)$) structure factors has been evaluated using the R-Factor [33, 63]. This is calculated using,

$$\boldsymbol{R = \frac{1}{M}\sum_i \frac{1}{n_Q(i)}\sum_Q [D_i(Q) - F_i(Q)]^2} \quad (7)$$

where, M is the number of datasets, $n_Q(i)$ is the number of Q values in the i^{th} dataset and the lower the value of R the closer the fit to the data. The R-Factor values for the glasses with compositions of x = 0.000, 0.250, 0.333, 0.500, 0.667 and 1.000 vary between 0.3-0.8 x 10^{-3} with an average of 0.6 x 10^{-3}. The R-factor calculated for the simulation of x = 0.750 is 0.7 x 10^{-3}. This level of agreement is within the range reported for data that has been explicitly fitted using EPSR, suggesting that the empirical potentials taken from the current work are transferable to other glass compositions in the $As_{40}Se_{60}$-$As_{40}S_{60}$ series. In future these potentials could be used to simulate the structure of other intermediate concentrations.

It should be stated that no attempt has yet been made to simulate non-stoichiometric compositions because the closest approach constraints, given in table 3, prevent the formation of homopolar bonds. This could be viewed as a limitation of this work but, as discussed in Section 3.2, many MD models of $As_{40}Se_{60}$ contain significantly more homopolar As-As bonds (~23%) [12, 18] than are expected from the analysis of spectroscopic techniques. This work demonstrates that models can be generated that are consistent with both X-ray and neutron data without the need for any homopolar bonding, and that the modelling approach used is robust enough to be a useful tool for predicting the structure of other glasses in the same glass series. The extension of this method to work for non-stochiometric compositions is already underway.

In conclusion, the use of MC-EPSR has advantages over T-EPSR for complex systems where there is insufficient data to guide the model. Firstly, simultaneously fitting data from a series of related glass compositions using neutron and X-ray data reduces the problem of the model being under constrained. The form of the total radial distribution functions are given in equations 1 and 2. They are comprised of a series of overlapping partial correlation functions, $S_{\alpha\beta}(Q)$, which must be deconvoluted to fully determine the structure of the glass. We have demonstrated that, for a complex glass with strongly overlapping $S_{\alpha\beta}(Q)$ and only weak scattering contrast, T-EPSR (combining neutrons and X-rays to vary the scattering lengths, b, that determine the intensity of each partial) is inadequate. MC-EPSR refines one set of potentials against a series of glasses to give contrast in the concentration of each of the elements, c as well b. In doing so, significantly more data sets are provided to guide the fit and ensure that the model more closely matches the real glass structures. The second advantage of this methodology is that it is predictive. MD and MC modelling methods use interatomic potentials to calculate the structure of a material, and are therefore predictive but have not been compared to experimental data, while RMC generates models that are more closely related to the measured structure of the glass, but are not predictive. Our approach combines these two methods. Experimental data for a series of samples is used to derive a series of interatomic potentials that accurately model the data and, as a result, we have developed a set of potentials that can be used to simulate the structure of a previously unmeasured glass reliably.

It is well know that there is a strong correlation between the structure of a material and its functional properties and so the applications of this methodology are wide ranging. All industrially relevant disordered materials, such as bioactive glasses, nuclear waste glasses, glasses for automotive and aerospace, components for fuel cells and optical glasses are complex multi component glasses and their structures are difficult to study by traditional methods for the reasons outlined above. However, these industries require high performance glasses that are optimised to give the correct physical properties for the applications. The ability to more reliably determine the structure of these glasses, and relate these structures to exhibited properties, as has been done in this study, will allow a more detailed understanding of structure-property relationships to be achieved. Furthermore, the ability to predict the structure of new glasses, and estimate their likely properties, will allow glass compositions to be optimised without the lengthy and costly trial and error stage of compositional development.

3.5. Interrogating the Model

One of the initially stated aims of this work was to develop a structural model for a series of $As_{40}Se_{60}$-$As_{40}S_{60}$ glasses that can be interrogated to determine structural origins for the glasses functional properties. For example, recently published results indicated that the glass transition temperature (Tg) and non-linear refractive indices (n_2) of the $As_{40}Se_{60}$-$As_{40}S_{60}$ series of glasses do not vary linearly with glass composition [11]. Both T_g and n_2 values for the ternary glasses were found to be more similar to the sulphide end member, $As_{40}S_{60}$, than $As_{40}Se_{60}$. Using direct analysis of neutron diffraction data, it has been suggested that this non-linear behaviour was due to a the non-linear change in the selenium-sulfur coordination number with increasing sulfur content [11]. This conclusion was based on the assumption that differences between a correlation function for a ternary glass and a suitably weighted sum of the end member compositions (i.e. $As_{40}Se_{30}S_{30}$ and $0.5As_{40}Se_{60}$+$0.5As_{40}S_{60}$) arise solely from Se-S correlations in the glass, which are unaccounted for in the weighted sum. An interrogation of the MC-EPSR simulations generated using the Lone-Pair configuration yields chalcogen-chalcogen coordination numbers that all vary linearly with concentration (See S.I. Figure S9). This observed behaviour casts doubt on the previously reported interpretation for the differences between the experimental correlation function for the ternary glasses and corresponding weighted sums calculated from the binary glass compositions [11]. The reported difference was observed in the second peak in the correlation function and, as stated previously in section 3.3, this peak is composed of a mix of all possible partial correlations; for the ternary glasses these comprise As-As, As-Se, As-S, Se-Se, S-S and Se-S. To state that a weighted sum of the As-Ch, As-As, Se-Se and S-S correlations in $As_{40}Se_{60}$ and $As_{40}S_{60}$ would generate the correct correlations for a ternary glass is likely to be an oversimplification of the structural rearrangements that occur on mixing chalcogen atoms together in the glass network.

An alternative explanation for the changes in functional properties that occur with composition in the $As_{40}Se_{60}$-$As_{40}S_{60}$ glass series can be found by examining the partial radial distribution functions ($g_{\alpha\beta}(r)$) produced by MC-EPSR for each of the chalcogen-chalcogen pairs. Figure 8 a and b show the partials for $g_{SS}(r)$, $g_{SSe}(r)$ and $g_{SeSe}(r)$ and show that there is no appreciable change in position of the nearest neighbour Ch…Ch peak with composition. The first peaks in the partials are centred at 3.39 Å for $g_{SS}(r)$, 3.42 – 3.45 Å for $g_{SSe}(r)$ and 3.60 – 3.66 Å for $g_{SeSe}(r)$, all within the region of the reported non-linear changes in $G(r)$ [11]. Figure 8a compares $g_{SS}(r)$ with $g_{SSe}(r)$ to show that the nearest neighbour distance for these two Ch-Ch interactions are within 0.06 Å. In contrast, selenium-selenium nearest neighbour distances are 0.21-0.27 Å longer than those for selenium-sulfur. This indicates that the mixed chalcogen-chalcogen interactions in the ternary glasses are more similar to S-S distances than Se-Se distances. It might be expected that this would result in a non-linear variation in the atomic number density but the data given in Table 1 show that this is not the case. This can be rationalised by considering the positions of the second peaks in the chalcogen-chalcogen $g_{ChCh}(r)$. Here, the differences between the three partials are reversed, with the positions of the second peaks in $g_{SSe}(r)$ and $g_{SeSe}(r)$ differing by only 0.06-0.09 Å (Figure 8b) , while the same peak position in $g_{SS}(r)$ is at a distance 0.12-0.15 Å shorter than the peak in $g_{SSe}(r)$ (Figure 8a). An alternative explanation for the non-linear variation in the non-linear refractive indices (n_2) measured for $As_{40}Se_{60}$-$As_{40}S_{60}$ glasses with increase selenium

content is the non-linear variation in the average Ch…Ch nearest neighbour distance. The similarity between the Se…S and S…S distances result in an average Ch…Ch separation in the ternary glasses that varies non-linearly with composition and is weighted to be more similar to that of $As_{40}S_{60}$ than $As_{40}Se_{60}$. Figure 8c shows the average Ch…Ch distance for atoms within the nearest neighbour coordination shell (here defined as being within 4 Å of each other) along with the corresponding variation in n_2 and the two parameters demonstrate similar trends with composition. Indeed, a linear relationship is demonstrated in Figure 8d. These results indicate that the conclusions of Barney *et al.* [11], which postulate that the chalcogen-chalcogen environment is correlated with non-linear refractive index, n_2, in the $As_{40}Se_{60}$-$As_{40}S_{60}$ glass system, are qualitatively correct. However, MC-EPSR simulations suggest that it is the relative distance between chalcogen atoms, rather than their coordination number, that leads to the macroscopic property changes with increased selenium content.

4. Conclusions

The structure of a series of $x As_{40}Se_{60}$-(1- x)$As_{40}S_{60}$ glasses where x = 1.000, 0.667, 0.500, 0.333, 0.250 and 0.000 has been investigated using a combination of neutron and X-ray diffraction along with Monte Carlo simulations. From the analysis of the simulated structures it was found that one neutron diffraction and one X-ray diffraction experiment was insufficient to constrain the Monte Carlo model for an individual glass composition. We have, therefore, used a multi-composition refinement procedure (MC-EPSR) to provide one set of interatomic potentials that are consistent with the experimental data for all of the compositions. Through the combination of MC-EPSR and minimal constraints we have produced a set of interatomic potentials that are consistent with experimental techniques and are transferable to new glass compositions. In agreement with previous glass structure studies [27-28] we find that including a lone-pair is required to constrain the model to the expected interatomic arrangement and coordination numbers. Investigation of the structures taken from the MC-EPSR analysis of the arsenic-sulfur-selenium glasses suggests that the changes with composition of the non-linear refractive indices, n_2, can be attributed to the distances between chalcogen atoms in the glass. Se…S distances are very similar to those of S…S, while Se…Se atoms distances tend to be ~0.2 Å longer. When the weighted partial radial distribution functions are added, the average Ch…Ch distance changes non-linearly with $As_{40}Se_{60}$ content correlating with the changes observed in n_2.

Supporting Information

Supporting information includes: Experimental neutron and X-ray data for each glass composition shown with traditional EPSR simulations. The As-Ch partial correlation functions for each glass composition produced by traditional EPSR simulations. Experimental neutron and X-ray data for each glass composition shown with multi-component EPSR simulations without dummy lone-pair atoms. The As-Ch partial correlation functions for each glass composition produced by multi-component EPSR simulations without dummy lone-pair atoms. Experimental neutron and X-ray data for each glass composition shown with multi-component EPSR simulations with dummy lone-pair atoms. The As-Ch partial correlation functions for each glass composition produced by multi-component EPSR simulations with dummy lone-pair atoms. The angular distribution of arsenic atoms around each chalcogen atom, along with the mean, modal and standard deviations for the bond angles, for each glass composition produced by multi-component EPSR simulations with dummy lone-pair atoms. The mean (black crosses) and modal (red circles) averages and standard deviations for bond angles. The partial correlation functions generated using Lone-Pair MC-EPSR for $As_{40}S_{60}$, $As_{40}S_{30}Se_{30}$ and $As_{40}Se_{60}$. The chalcogen-chalcogen coordination numbers, n_{ChCh}, for each glass composition calculated using the Lone Pair MC-EPSR simulations.

Acknowledgements

Experiments at the ISIS Pulsed Neutron and Muon Source were supported by a beamtime allocation (RB1120102) from the Science and Technology Facilities Council. We also thank Diamond Light Source for access to Beamline I15. We would like to thank Prof. Micoulaut for the use of his data (shown in Figure 7). Dr D. Bowron and Professor A. Soper are also thanked for useful discussions regarding the implementation of EPSR for glass systems. Finally ERB would like to that the University for Nottingham for the award of a Dean of Engineering Fellowship, which funded this work.

Tables

Table 1. The density (ρ) and atomic composition of the $x As_{40}Se_{60}$-(1- x)$As_{40}S_{60}$ glasses that are used as parameters for all simulations.

x	ρ (atoms Å^{-3})	Composition		
		Arsenic No.	Sulfur No.	Selenium No.
0.000	0.0391	2,000	3,000	0
0.250	0.0384	2,000	2,250	750
0.333	0.0379	2,000	2,000	1,000
0.500	0.0372	2,000	1,500	1,500
0.667	0.0363	2,000	1,000	2,000
1.000	0.0354	2,000	0	3,000

Table 2. Lennard-Jones parameters, Coulomb charges and masses that define the reference potentials for each of the MC-EPSR configurations. Here, As is used for the atomic configuration and As' and qAs are used for the lone pair configuration.

Label	ε (kJ mol^{-1})	σ (Å)	q (e)	Mass (a.m.u)
As	0.80	2.45	0.60	75.00
S	0.80	2.35	-0.40	32.00
Se	0.80	2.55	-0.40	79.00
As'	0.80	2.45	0.90	37.50
qAs	0.00	0.00	-0.30	37.50

Table 3. Minimum atomic separations (Rmin) used for the MC-EPSR simulations. Pairs not listed have Rmin = 0.90 Å.

Atom 1	Atom 2	Rmin (Å)
As	As	2.80
As	S	1.80
As	Se	1.80
qAs	S	2.30
qAs	Se	2.40
S	S	2.40
S	Se	2.50
Se	Se	2.60

Table 4. The average coordination numbers of chalcogen atoms around arsenic in $As_{40}S_{60}$ and $As_{40}Se_{60}$ calculated from the MC-EPSR simulations with Atomic and Lone-Pair configurations. The associated standard deviations (s.d.) for each of the EPSR setups is also given.

	$As_{40}S_{60}$		$As_{40}Se_{60}$	
Configuration	As-S Coord	As-S s.d.	As-Se Coord	As-Se s.d.
Atomic	3.20992	0.68409	3.08379	0.71266
Lone Pair	3.00291	0.34752	2.97353	0.27081

Table 5. The percentage of arsenic atoms coordinated by 2, 3 and 4 chalcogen atoms in the MC-EPSR simulations with Atomic and Lone-Pair configurations.

x	Atomic MC-EPSR			Lone-Pair MC-EPSR		
	2	**3**	4	2	**3**	4
0.000	12.0	**53.9**	32.4	4.5	**89.4**	6.2
0.250	11.5	**53.7**	33.2	4.9	**87.9**	7.2
0.333	11.4	**50.0**	37.0	4.1	**90.7**	5.2
0.500	12.6	**54.0**	32.1	3.9	**91.1**	5.1
0.667	14.3	**52.6**	31.6	3.9	**91.6**	4.5
1.000	17.7	**53.3**	27.8	4.8	**92.4**	2.9

Figures

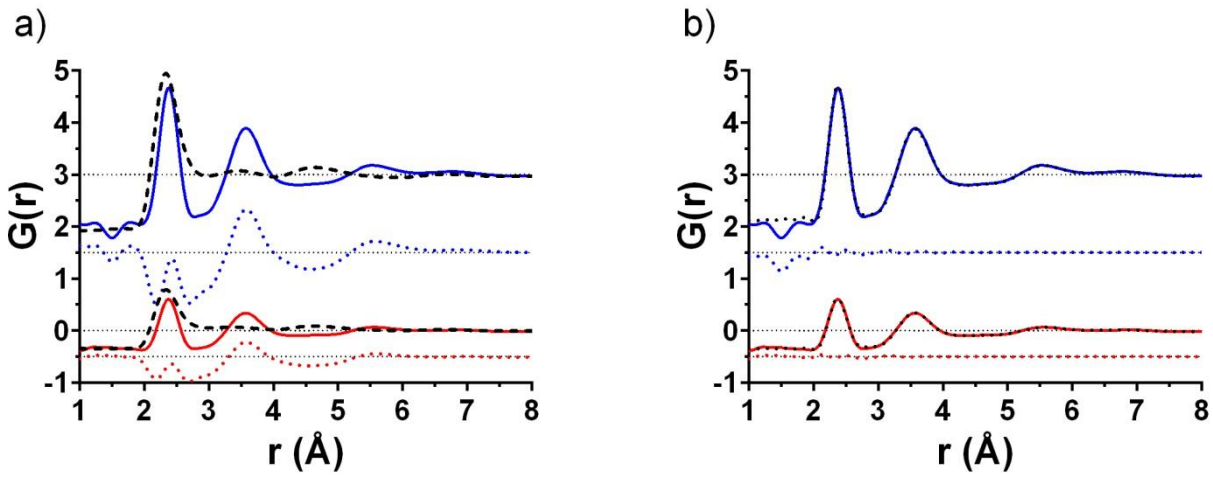

Figure 1: Experimental neutron (solid red) and X-ray (solid blue) radial distribution functions, G(r), for $As_{40}Se_{30}S_{30}$ plotted with those produced from the T-EPSR simulations using a) reference potentials only (black dashed lines) and b) reference and empirical potentials (dotted black line). The residuals are shown using coloured dotted/dashed lines and the X-ray G(r)s are shifted to aid clarity.

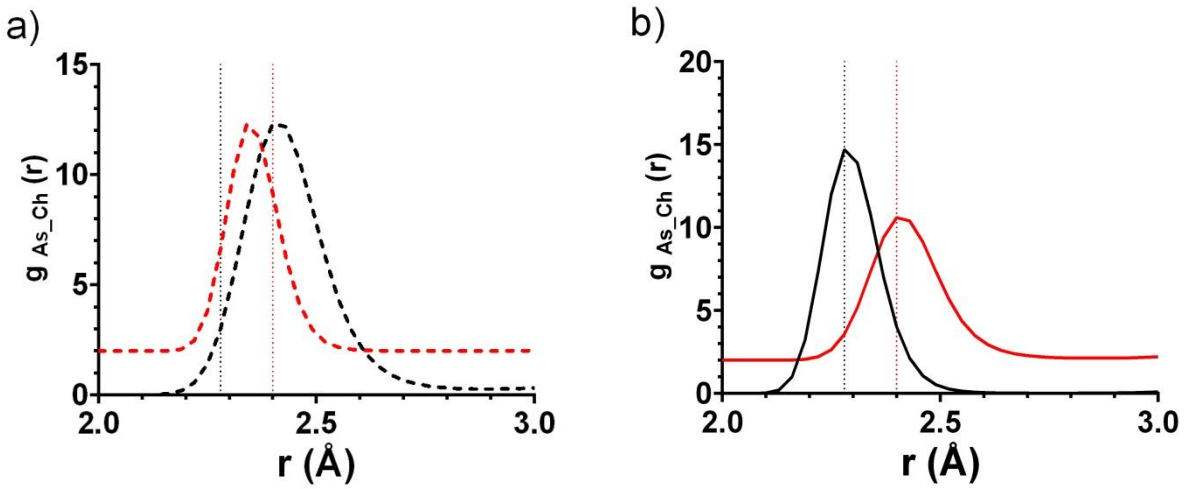

Figure 2**:** Partial radial distribution functions, $g_{As\text{-}Ch}(r)$, for arsenic-sulphur (black) and arsenic-selenium (red) correlations taken from (a) T-EPSR and (b) an Atomic MC-EPSR simulation of $As_{40}S_{30}Se_{30}$. The vertical black dotted lines at 2.28 Å indicate the position of the first peak in the G(r) for $As_{40}S_{60}$ and the red vertical dotted lines at 2.40 Å indicate the position of the first peak in the G(r) for $As_{40}Se_{60}$.

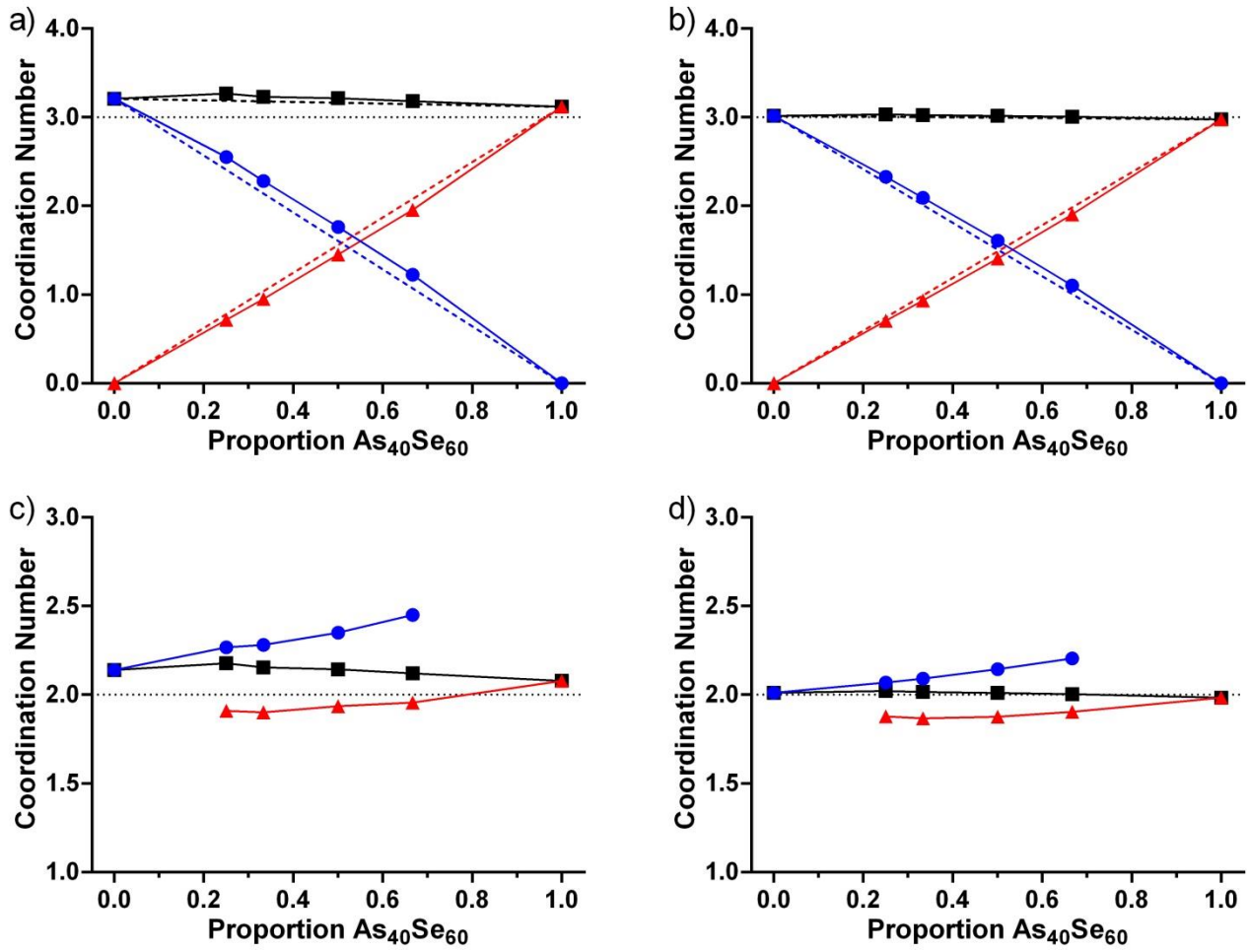

Figure 3. n_{AsCh}, n_{AsS} and n_{AsSe}, for each glass composition obtained using the a) Atomic and b) Lone-Pair configurations are plotted with the corresponding values for n_{ChAs}, n_{SAs} and n_{SeAs} obtained using the c) Atomic and b) Lone-Pair configurations. Dotted lines indicate the expected coordination numbers and dashed lines are a linear fit to the extreme concentrations.

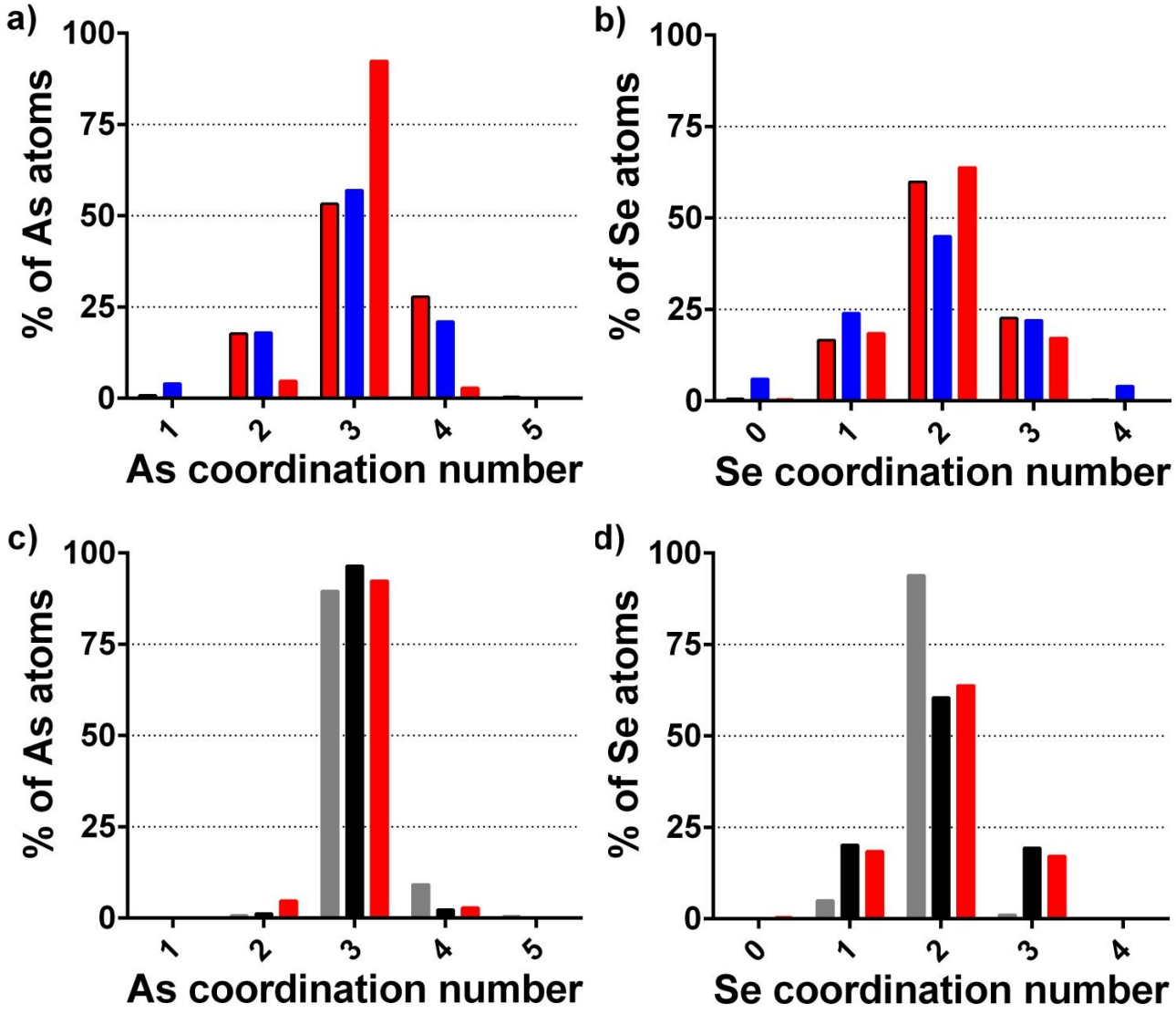

Figure 4. The distribution of arsenic (a and c) and selenium (b and d) coordination numbers taken from the MC-EPSR analysis of $As_{40}Se_{60}$ are shown with results from previously published simulations. The data from the MC-EPSR simulation using an Atomic configuration is shown in red with a black outline while the Lone-Pair model is shown as a solid red bar. The distributions from Mauro and Varshneya [15] (blue), Bauchy and Micoulaut [12] (grey) and Li and Drabold [18-19](black) are shown for comparison.

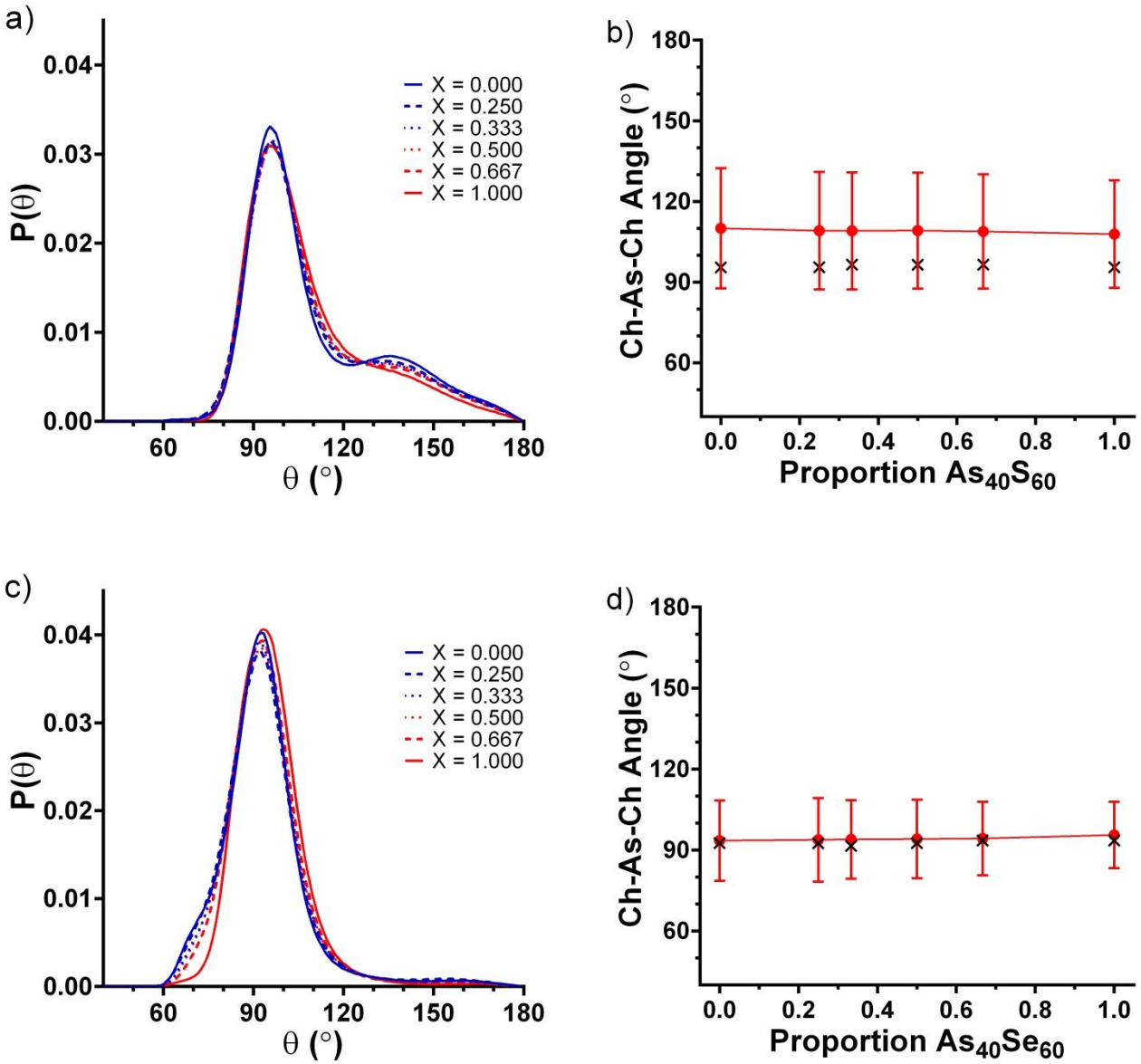

Figure 5. The angular distribution of chalcogen atoms around each arsenic atom (Ch-As-Ch) taken from the a) Atomic and c) Lone-Pair configurations for MC-EPSR. The mean (black crosses) and modal (red circles) averages and standard deviations for bond angles in these two configurations are given in b) and d) respectively.

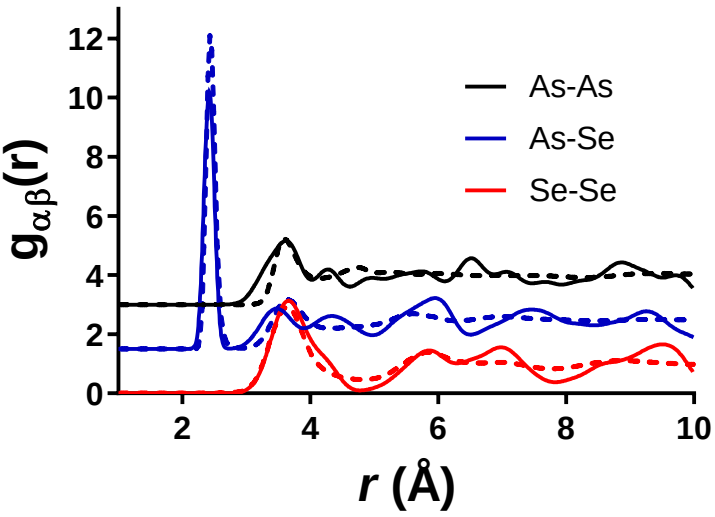

Figure 6: A comparison of the partial correlation functions, $g_{\alpha\beta}(r)$, obtained from the lone pair simulation of amorphous As_2Se_3 (solid lines) with those generated for crystalline As_2Se_3 (dashed lines).

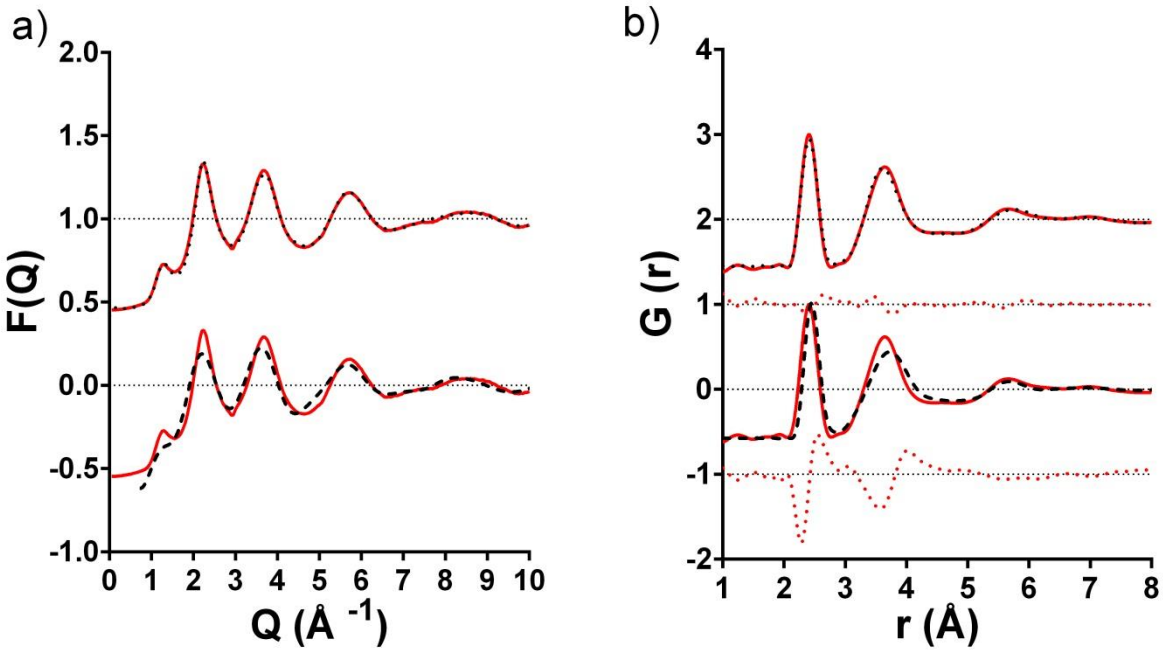

Figure 7. Experimental a) $F(Q)$ and b) $G(r)$ for $As_{40}Se_{60}$ [11] (solid red line) plotted with the simulated structure factors and $G(r)$s generated using the MC-EPSR Lone-Pair configuration (black dotted line) and MD [12] (black dashed line). The data have been shifted vertically to aid clarity. The red dotted line in (b) shows the difference between experiment and simulation.

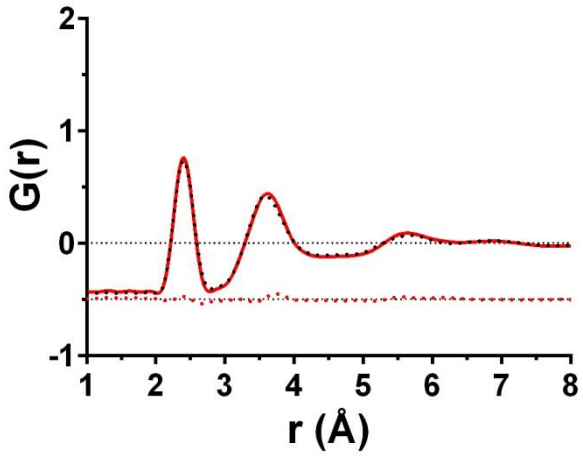

Figure 8 Experimental $G(r)$ for $As_{40}Se_{45}S_{15}$ (solid red line) shown with the predicted $G(r)$ (black dotted line) produced using the potentials obtained from MC-EPSR using the Lone-Pair configuration for six As-Se-S glass compositions. The red dotted line is the residual.

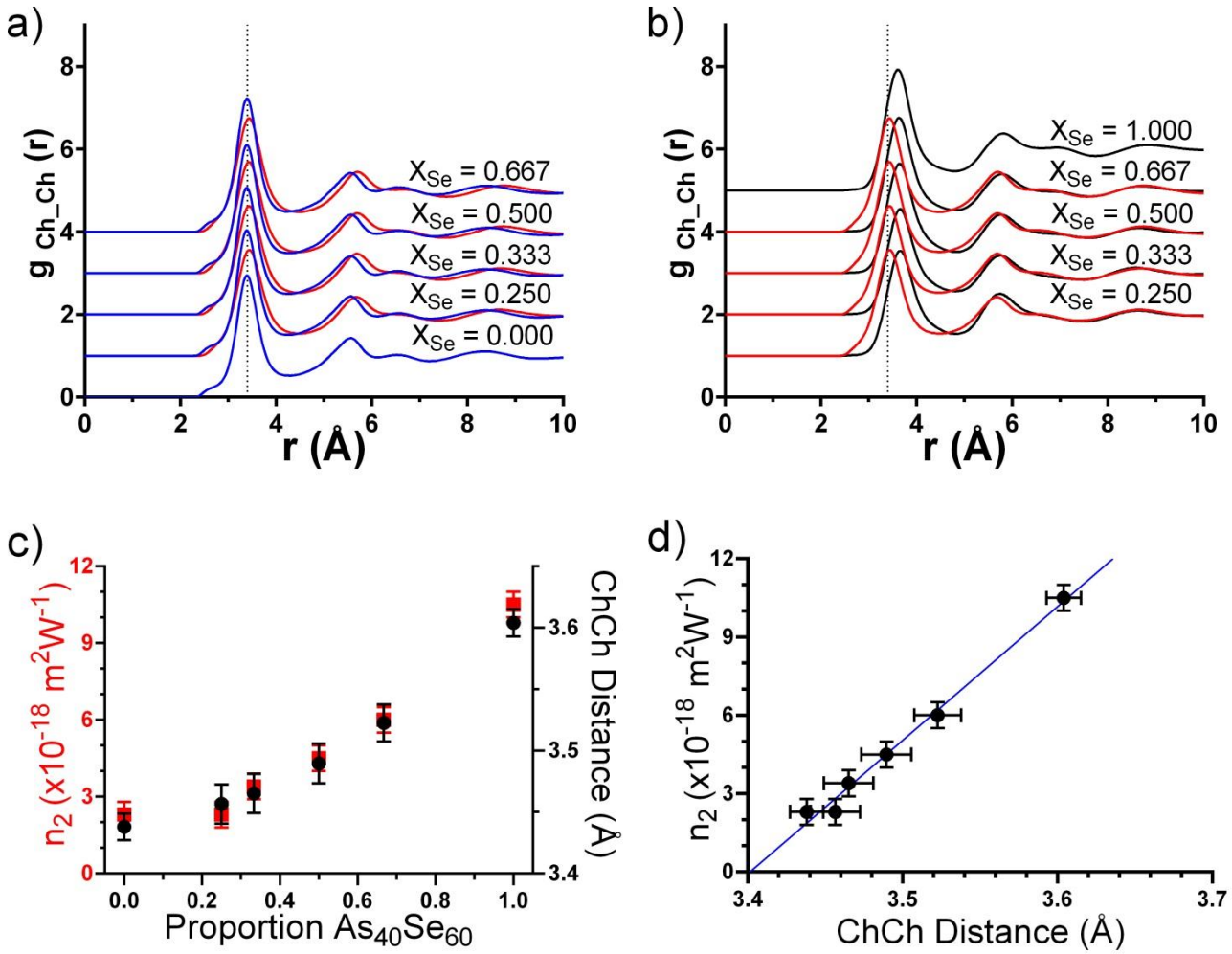

Figure 9 The chalcogen-chalcogen partial radial distribution functions, $g_{ChCh}(r)$, taken from MC-EPSR using the Lone-Pair configuration; a) $g_{SS}(r)$ (blue), $g_{SSe}(r)$ (red) and b) $g_{SSe}(r)$ (red) and $g_{SeSe}(r)$ (black). c) the average chalcogen-chalcogen separation (black) and the non-linear refractive indices, n_2 (red) [11]. d) n_2 plotted against the average chalcogen-chalcogen separation with a linear fit shown in blue.

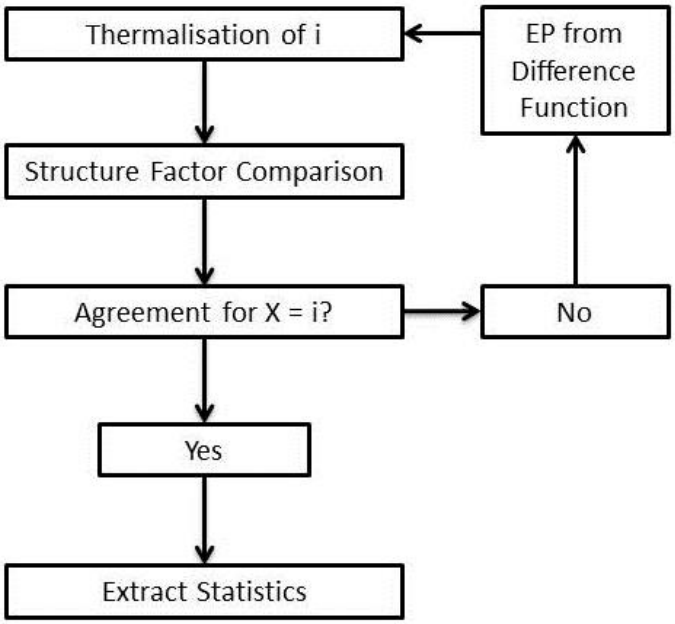

Scheme 1: Traditional EPSR begins with a Monte Carlo simulation of the structure of the system being studied (i). The simulated structure factor is then compared to the experimental data and a difference function is calculated. An empirical potential is produced based on this function and is added to the reference potentials. This is repeated until the simulation is in agreement with the experiment. An ensemble of structures is extracted once agreement is reached.

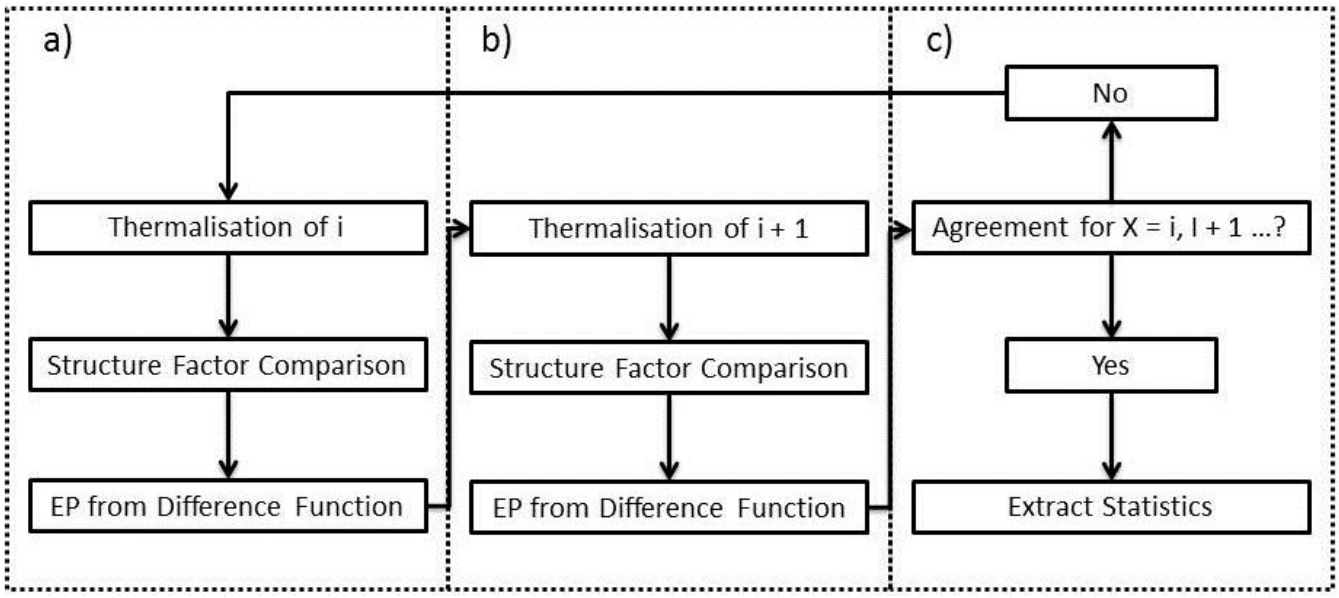

Scheme 2: Multi Composition EPSR begins is a similar way to traditional EPSR. Reference potentials are used to drive a simulations of systems X = i, i+1, … n to equilibrium. The difference between the simulation and experimental structure factors is then calculated and used to produce an empirical potential, which is then used to modify the potentials for system i+1. The potentials are then further modified and passed to composition i+2, repeated for each of the systems being studied until all of the simulated structure factors are in agreement with the relevant experimental data.

6. References

1. Seddon, A. B., *Phys Status Solidi B* **2013**, *250*, 1020-1027.

2. Seddon, A. B., *Int J Appl Glass Sci* **2011**, *2*, 177-191.

3. Grant, W. B.; Kagann, R. H.; Mcclenny, W. A., *J Air Waste Manage* **1992**, *42*, 18-30.

4. Medhurst, L. J., *Journal of Chemical Education* **2005**, *82*, 278-281.

5. Wong, P. T. T.; Goldstein, S. M.; Grekin, R. C.; Godwin, T. A.; Pivik, C.; Rigas, B., *Cancer Res* **1993**, *53*, 762-765.

6. Lachenmeier, D. W., *Food Chem* **2007**, *101*, 825-832.

7. Cardinal, T.; Richardson, K. A.; Shim, H.; Schulte, A.; Beatty, R.; Le Foulgoc, K.; Meneghini, C.; Viens, J. F.; Villeneuve, A., *J Non-Cryst Solids* **1999**, *256*, 353-360.

8. Drabold, D. A.; Li, J.; Tafen, D., *J. Phys.: Condens. Matter* **2003**, *15*, S1529-S1536.

9. Harbold, J. M.; Ilday, F. O.; Wise, F. W.; Sanghera, J. S.; Nguyen, V. Q.; Shaw, L. B.; Aggarwal, I. D., *Opt Lett* **2002**, *27*, 119-121.

10. Lin, F. Y.; Gulbiten, O.; Yang, Z. Y.; Calvez, L.; Lucas, P., *J Phys D Appl Phys* **2011**, *44* 045404.

11. Barney, E. R.; Abdel-Moneim, N. S.; Towey, J. J.; Titman, J.; McCarthy, J. E.; Bookey, H. T.; Kar, A.; Furniss, D.; Seddon, A. B., *Phys Chem Chem Phys* **2015**, *17*, 6314-6327.

12. Bauchy, M.; Micoulaut, M., *J. Non-Cryst. Solids* **2013**, *377*, 34-38.

13. Fabian, M.; Svab, E.; Pamukchieva, V.; Szekeres, A.; Todorova, K.; Vogel, S.; Ruett, U., *J Phys Chem Solids* **2013**, *74*, 1355-1362.

14. Kaban, I.; Jovari, P.; Wagner, T.; Frumar, M.; Stehlik, S.; Bartos, M.; Hoyer, W.; Beuneu, B.; Webb, M. A., *J. Phys.: Condens. Matter* **2009**, *21* 395801.

15. Mauro, J. C.; Varshneya, A. K., *J Non-Cryst Solids* **2007**, *353*, 1226-1231.

16. Shimojo, F.; Hoshino, K.; Zempo, Y., *J. Phys. Soc. Jap.* **2005**, *74*, 621-625.

17. Simdyankin, S. I.; Elliott, S. R.; Hajnal, Z.; Niehaus, T. A.; Frauenheim, T., *Phys. Rev. B* **2004**, *69* 144202.

18. Li, J.; Drabold, D. A., *Phys. Rev. B* **2000**, *61*, 11998-12004.

19. Li, J.; Drabold, D. A., *Phys Rev B* **2001**, *64*, 104206.

20. Hosokawa, S.; Koura, A.; Berar, J. F.; Pilgrim, W. C.; Kohara, S.; Shimojo, F., *Epl-Europhys Lett* **2013**, *102*, 66008.

21. Aniya, M.; Shimojo, F., *J Non-Cryst Solids* **2006**, *352*, 1510-1513.

22. Inui, M.; Kajihara, Y.; Kimura, K.; Fukumaru, T.; Matsuda, K.; Yao, M., *J Non-Cryst Solids* **2013**, *366*, 22-29.

23. Zhu, X. F.; Chen, L. F., *Physica B* **2008**, *403*, 3302-3306.

24. Gjersing, E. L.; Sen, S.; Aitken, B. G., *J. Phys. Chem. C* **2010**, *114*, 8601-8608.

25. McGreevy, R. L.; Pusztai, L., *Mol Simulat* **1988**, *1*, 359-367.

26. Fabian, M.; Svab, E.; Pamukchieva, V.; Szekeres, A.; Vogel, S.; Ruett, U., *J Phys Conf Ser* **2010**, *253* 012053.

27. Alderman, O. L. G.; Hannon, A. C.; Holland, D.; Feller, S.; Lehr, G.; Vitale, A. J.; Hoppe, U.; von Zimmerman, M.; Watenphul, A., *Physical Chemistry Chemical Physics* **2013**, *15*, 8506-8519.

28. Barney, E. R.; Hannon, A. C.; Laorodphan, N.; Holland, D., *J Phys Chem C* **2011**, *115*, 14997-15007.

29. Soper, A. K., *Chemical Physics* **1996**, *202*, 295-306.

30. Towey, J. J.; Soper, A. K.; Dougan, L., *Faraday Discuss* **2013**, *167*, 159-176.

31. Soper, A. K., *J Phys-Condens Mat* **2011**, *23*, 365402.

32. Bowron, D. T., *Mater Sci Eng B-Adv* **2008**, *149*, 166-170.

33. Soper, A. K., *J. Phys.: Condens. Matter* **2007**, *19* 41508.

34. Weigel, C.; Cormier, L.; Calas, G.; Galoisy, L.; Bowron, D. T., *J. Non-Cryst. Solids* **2008**, *354*, 5378-5385.

35. Bernasconi, A.; Dapiaggi, M.; Pavese, A.; Bowron, D. T.; Imberti, S., *J. Phys. Chem. B* **2012**, *116*, 13114-13123.

36. Hannon, A. C., *Nucl Instrum Meth A* **2005**, *551*, 88-107.

37. Soper, A. K., *RAL Technical Reports* **2011**, RAL-TR-2011-013.

38. Hannon, A. C.; Howells, W. S.; Soper, A. K., *Inst Phys Conf Ser* **1990**, *107*, 193-211.

39. Hammersley, A. P., *ESRF Internal Report* **1998**, *ESRF98HA01T*.

40. Hammersley, A. P.; Svensson, S. O.; Hanfland, M.; Fitch, A. N.; Hausermann, D., *High Pressure Research* **1996**, *14*, 235-248.

41. Skinner, L. B.; Benmore, C. J.; Parise, J. B., *Nucl Instrum Meth A* **2012**, *662*, 61-70.

42. Kroghmoe, J., *Acta Crystallogr* **1956**, *9*, 951-953.

43. Norman, N., *Acta Crystallogr* **1957**, *10*, 370-373.

44. Soper, A. K.; Barney, E. R., *J Appl Crystallogr* **2011**, *44*, 714-726.

45. Lorch, E., *J. Phys. C* **1969**, *2*, 229.

46. Soper, A. K., *Mol. Phys.* **2001**, *99*, 1503-1516.

47. Soper, A. K., *Phys Rev B* **2005**, *72* 104204.

48. Soper, A. K., *J Phys-Condens Mat* **2010**, *22* 404210.

49. Rhys, N. H.; Soper, A. K.; Dougan, L., *J Phys Chem B* **2012**, *116*, 13308-13319.

50. Hayes, R.; Imberti, S.; Warr, G. G.; Atkin, R., *Phys Chem Chem Phys* **2011**, *13*, 3237-3247.

51. Busch, S.; Pardo, L. C.; O'Dell, W. B.; Bruce, C. D.; Lorenz, C. D.; McLain, S. E., *Phys Chem Chem Phys* **2013**, *15*, 21023-21033.

52. Sillren, P.; Swenson, J.; Mattsson, J.; Bowron, D.; Matic, A., *J Chem Phys* **2013**, *138* 124501.

53. Brese, N. E.; Okeeffe, M., *Acta Crystallogr B* **1991**, *47*, 192-197.

54. Stergiou, A. C.; Rentzeperis, P. J., *Z Kristallogr* **1985**, *173*, p185-p191.

55. Mullen, D. J. E.; Nowacki, W., *Z Kristallogr* **1972**, *136* 46-56.

56. Gillespie, R. J., *Chem. Soc. Rev.* **1992**, *21*, 59-69.

57. Hannon, A. C.; Barney, E. R.; Holland, D.; Knight, K. S., *J Solid State Chem* **2008**, *181*, 1087-1102.

58. Hannon, A. C., Rutherford Appleton Laboratory: RAL-93-063, **1993**.

59. Stergiou, A. C.; Rentzeperis, P. J., *Z Kristallogr* **1985**, *173*, 185-191.

60. Xin, S. Q.; Liu, J.; Salmon, P. S., *Phys Rev B* **2008**, *78* 064207.

61. Li, W. Y.; Seal, S.; Rivero, C.; Lopez, C.; Richardson, K.; Pope, A.; Schulte, A.; Myneni, S.; Jain, H.; Antoine, K.; Miller, A. C., *J Appl Phys* **2005**, *98* 053503.

62. Georgiev, D. G.; Boolchand, P.; Jackson, K. A., *Phil. Mag.* **2003**, *83*, 2941-2953.

63. Towey, J. J.; Soper, A. K.; Dougan, L., *Phys. Chem. Chem. Phys.* **2011**, *13*, 9397-9406.

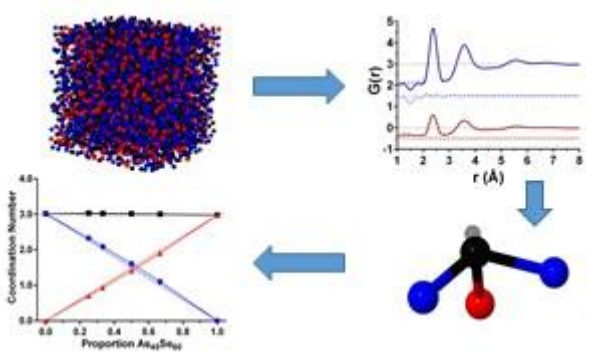
G(r)
r (Å)
Coordination Number
Proportion $As_{40}Se_{60}$